Materials Advances

ROYAL SOCIETY OF CHEMISTRY

PAPER

View Article Online
View Journal | View Issue

Cite this: *Mater. Adv.*, 2024, 5, 2926

Synthesis of 20-nm-sized CoAl-LDH nanoparticles modified with folic acid for enhanced cancer cell targeting†

Yasuaki. Tokudome, *[ab] Akiko Obata, *[c] Nijika Kitagawa,[b] Katsumi Nagatsuka,[c] Eisuke Gorai,[c] Yui Maehashi,[a] Yojiro Kishida,[a] Hidenobu Murata,[ab] Atsushi Nakahira[ab] and Toshihiro Kasuga[c]

Received 27th November 2023,
Accepted 1st February 2024

DOI: 10.1039/d3ma01053h

rsc.li/materials-advances

Nanomaterials with a highly exposed surface are a topic of growing interest for their application in chemodynamic therapy (CDT). In this study, we have demonstrated a facile synthesis of 20-nm-sized CoAl layered double hydroxide (LDH) nanoparticles modified with folic acid. The surface modification of the nanoparticles with folic acid was performed using an electrostatic interaction between the glutamate moiety of folic acid and CoAl LDH. The modification with FA was found to be advantageous for the controlled dissolution of LDH nanoparticles in a pH-responsive manner. Additionally, cell culture tests suggest that the materials exhibit targeting properties towards cancer cells for the enhancement of cellular uptake. The unique nanometric CoAl-LDH-based material is a good candidate to fill the gap between delaminated sheets with a single layer thickness and large well-crystallized LDHs and is promising as a Co-based nanomaterial for CDT application.

1. Introduction

Increasing attention is being focused on chemodynamic therapy (CDT), which is an *in situ* treatment to destroy cancer cells using an oxidation process.[1,2] Apoptosis of cancer cells is induced by reactive hydroxyl radicals (•OH) generated through the oxidation process (Fenton reaction),[3] with the aid of catalysts, such as Fe(II) and non-ferrous transition metal cations of, Ce^{3+}, Cu^{2+}, and Co^{2+}.[4] Nanomaterials that quickly dissolve and release these non-ferrous transition metals are especially attractive because they exhibit additional advantages to enhance the effect of CDT by increasing the sensitivity of cancer cells toward the oxidation, through the depletion of glutathione (GSH).[3,5–10]

Layered double hydroxides (LDHs) possess a general formula of $[M_{1-x}^{2+}M_x^{3+}(OH)_2][A_{x/n}^{n-}\cdot mH_2O]$, where M^{2+} and M^{3+} are di- and trivalent cations, and A^{n-} is an anion. The tunable and distinctive properties of LDHs are surface basicity, adsorptive nature, anion exchangeability, and biological and environmental compatibilities.[11,12] The versatility of the chemical composition of LDH, and the resultant fine-tuning of chemical/physical properties are advantageous features for modalities of therapy, including CDT. The use of nanometric LDHs, especially nanosheets, with a highly exposed surface is a topic of growing interest because of their quick response to the tumor microenvironment. For example, CoMn-LDH ultrathin nanosheets,[7,13] MgFe-based LDH nanohybrids,[14] Ce-doped CuAl LDH nanosheets,[15] CuFe-LDH nanosheets,[16] and MnMgFe-LDH nanocomposites,[17] and FeMn LDH nanosheets[18] were demonstrated to provide abundant reactive sites to accelerate heterogeneous Fenton-like reactions as well as GSH depletion.

LDH nanosheets with an atomic layer thickness are prepared by delaminating well-crystallized LDH bulk crystals. On the other hand, strong electrostatic interactions between layers and rigid hydrogen-bonding networks in interlayers of LDH crystals make them more difficult to exfoliate compared to other clay silicates, such as montmorillonite and LAPONITE®.[19,20] This is the reason why hydroxide nanosheets are normally obtained in small mass as a suspension at low concentrations; otherwise, they easily aggregate and restack to form large particles in polar solvents.[19] Troublesome reaction steps are required for the preparation of LDH nanosheets as a dried powder, limiting their synthesis even on the gram scale.

Recently, we reported the synthesis of a concentrated colloidal dispersion of CoAl LDH nanoparticles (40 g L^{-1}) with a lateral size of <20 nm showing a relatively low aspect ratio.[21] The material can be obtained through a one-pot synthesis at

[a] *Department of Materials Science, Osaka Prefecture University, 1–1 Gakuen-cho, Naka-ku, Sakai 599–8531, Japan. E-mail: tokudome@mtr.osakafu-u.ac.jp*
[b] *Department of Materials Science, Osaka Metropolitan University, 1–1 Gakuen-cho, Naka-ku, Sakai 599–8531, Japan. E-mail: tokudome@omu.ac.jp*
[c] *Division of Advanced Ceramics, Nagoya Institute of Technology, Gokiso-cho, Showa-ku, Nagoya 466–8555, Japan. E-mail: obata.akiko@nitech.ac.jp*

† Electronic supplementary information (ESI) available. See DOI: https://doi.org/10.1039/d3ma01053h

room temperature under an ambient atmosphere, allowing for bulk synthesis. The size of the CoAl LDH nanoparticles is smaller compared to ones prepared though general synthesis strategies such as the co-precipitation route (particle size: 80–250 nm),[22,23] the urea hydrolysis route (particle size: 2–8 μm),[24–28] and the glycidol alkalization route (2–12 μm).[29] Thanks to their morphological features, the CoAl LDH nanoparticles reportedly exhibit a 47 times higher rate of degradation of dye molecules and 13.6 times higher specific surface area compared to standard CoAl LDH with micrometer size. These unique CoAl LDH nanoparticles are good candidates to fill the gap between the delaminated nanosheets and the large well-crystalized LDHs, and are promising as a Co-based nanomaterial for CDT application. To this end, modification of the reactive surface of the nanoparticles to impart controlled dissolution of Co^{2+} ions towards the targeted therapy of cancer cells is required to be established.

Herein, we have developed 20-nm-sized CoAl LDH nanoparticles modified with folic acid, exhibiting enhanced targeted properties and a controlled release of Co^{2+} ions under a tumor microenvironment in a pH-responsive manner. The surface modification of the nanoparticles with folic acid was found to allow for controlled dissolution of LDH nanoparticles as well as to impart the targeting property towards cancer cells for the enhancement of cellular uptake. The controlled release of Co^{2+} can be explained by the fact that FA exhibits a relatively low solubility in neutral and acidic pH ranges,[30,31] and complexation of Co^{2+} with FA retards the dissolution of Co^{2+} from the surface. As a result, the FA modified CoAl LDH exhibits a higher toxicity to cancer cells compared to normal cells because, in addition to the targeting properties, the onset of dissolution of nanoparticles is induced by a trace difference of pH corresponding to the one between cancer and normal cells. It should be underlined that the properties that emerged from the modification are specific to the nanoscale features of the particles. A negligible amount of the modification could be made on well-crystallized CoAl LDH platelets through the present easy scheme. Although further assessment is still needed, the nanomaterial obtained here has potential to be used as a nano agent and nano building blocks for emerging therapeutic modalities including CDT.

2. Experimental

2.1. Chemicals

Cobalt(II) chloride hexahydrate ($CoCl_2{\cdot}6H_2O$, 99.0%), aluminum chloride hexahydrate ($AlCl_3{\cdot}6H_2O$, 98.0%), ethanol (EtOH, 99.5%), acetylacetone (acac, 99.0%), and dimethyl sulfoxide (DMSO, 99.0%) were purchased from FUJIFILM Wako Pure Chemicals Corporation. Propylene oxide (PO, ≥99%) was purchased from Sigma-Aldrich Co. LLC. Folic acid (FA, ≥98%) was purchased from Tokyo Chemical Industry Co., Ltd. All the chemicals were used as received.

2.2. Synthesis of CoAl LDH nanoparticles (CoAl-LDH)

CoAl LDH nanoparticles were prepared *via* a synthesis route modified from a previous report;[21] the chemical composition was changed such that CoAl LDH can be obtained as a stable suspension with a low viscosity. $CoCl_2{\cdot}6H_2O$ (0.445 g; 1.87 mmol) and $AlCl_3{\cdot}6H_2O$ (0.226 g; 0.935 mmol) were dissolved in a mixture of ethanol (3.00 mL) and ion-exchanged water (2.00 mL). Acetylacetone (acac) (97.5 μL; 0.935 mmol) was added to this mixture and stirred for 30 min in a closed container. Then, propylene oxide (PO) (2.62 mL; 37 mmol) was added and further stirred for 1 min to yield a homogenous solution. Stirring was stopped and the container was placed at 25 °C under a static condition for 96 h. The thus obtained suspension was freeze-dried (FDS-1000, EYELA), and heat-treated at 250 °C for 1h, to yield powdery LDH nanoparticles. Hereafter, this sample is called CoAl-LDH (see Fig. S1 for the TEM image and particle size distribution, ESI†). The average diameter of CoAl-LDH, estimated from the image, is 18 nm. As a comparison, referential LDH (Ref-CoAl-LDH) was also prepared according to a previous study.[32] The detailed results are described in the ESI.†

2.3. Synthesis of CoAl LDH nanoparticles modified with FA (CoAl-LDH-FA)

Folic acid (FA) (0.44 g; 1.0 mmol) was dissolved in 10 mL of dimethyl sulfoxide (DMSO), and further 100-times diluted with DMSO. 0.12 g of CoAl-LDH was dispersed in 15 mL of the diluted FA solution, followed by stirring for 72 h. The nanoparticles modified with FA were collected by centrifugation at 12 000 rpm, washed several times, and dried at 50 °C in air. Hereafter, this sample was called CoAl-LDH-FA. Note that the amount of FA (15 μmol) used for the modification corresponds to the one required to fully cover the surface of 0.12 g of LDH with a specific surface area of 136 $m^2\ g^{-1}$ (13 μmol), by assuming a polar surface area of FA (2.1×10^2 $Å^2$)[33] as the cross-sectional size.

2.4. Characterization

Zeta potential measurements were performed with ELSZ-DN2 (Otsuka Electronics Co., Ltd). The measurement was performed at pH = 7.4. 0.01 g of powdery sample was dispersed in 5 mL of H_2O containing small amount of 0.1 mol L^{-1} NaCl as an electrolyte. X-ray fluorescence spectroscopy (XRF; EDX-7000, Shimadzu Corporation) was employed to evaluate the Co/Al ratio of CoAl-LDH and CoAl-LDH-FA, based on the calibration curve method using standard reference materials. Inductively coupled plasma (ICP-AES) analysis (PS7800, Hitachi High-Tech Corporation) was performed to determine a concentration of metal species dissolved in phosphate buffer solution for various pH values. Sample powders were added to phosphate buffer solutions (0.1 mol L^{-1}, pH = 6.0, 6.4, 7.4, FUJIFILM Wako Pure Chemicals Corporation) at particle concentrations of 20, 30, and 50 ppm. The buffer solutions were placed at 37 °C in an incubator for 24 h. Then, the supernatant (15.0 mL) was collected by filtering undissolved particles, allowed to dry at 50 °C, and heat-treated at 500 °C for 1 h. 1 mol L^{-1} HNO_3 (15.0 mL) was added to dissolve and liquid to be analyzed was collected through a 0.2 μm syringe filter.

The crystalline nature of the samples was identified by powder X-ray diffraction (XRD; Mini Flex 600C, Rigaku Corporation)

using Cu Kα radiation (λ = 0.1540 nm) and a one-dimensional fast detector (D/tex Ultra2, Rigaku Corporation). The divergence slit was set at 0.625°. A Ni filter was used to remove Cu-K_β radiation. Fourier transform infrared (FT-IR) spectra of samples were recorded with a scan resolution of 1 cm^{-1} on a spectrophotometer (FT/IR-4600, JASCO Corporation). The sample powder was placed between KBr plates, pressed into a pellet, and subjected to measurements. N_2 adsorption–desorption isotherms at −196 °C were obtained on a volumetric gas adsorption apparatus (BELSORP-mini II, Microtrac BEL Corporation). Prior to the measurements, sample powders were pretreated at 200 °C under vacuum conditions overnight. Specific surface area (S_{BET}) was estimated using the Brunauer–Emmett–Teller (BET) method. Thermogravimetric-differential thermal analysis (TG-DTA; DTG-60H, Shimadzu Corporation) was carried out at a ramp rate of 10 °C min^{-1} in an air atmosphere to assess the thermal behaviour and chemical composition. Prior to the TG-DTA measurements, all the samples were washed with DMSO and dried at 50 °C. A transmission electron microscope (TEM; JEM-2000FX, JEOL Ltd) was used to observe the nanometric structure of the particles. A powder sample (1 mg) for TEM observation was dispersed in 15 mL of EtOH and the supernatant was dropped onto a Cu grid and allowed to dry. The particle size distribution was obtained from the images of more than 100 particles for each sample. Scanning electron microscope (SEM) observations were performed using a JCM-7000 instrument (JEOL Ltd).

2.5. Cell culture tests

DMEM (Gibco) and E-MEM (FUJIFILM Wako Pure Chemicals Corporation) after supplementing 10 vol% of fetal bovine serum and 1 vol% of penicillin/streptomycin were used for culturing NIH3T3 and HeLa, respectively. The culture media containing CoAl-LDH-FA or CoAl-LDH were prepared by adding a water containing each LDH sample into the culture medium, followed by 24 h-keeping in a humidified incubator with 5% CO_2 for pH control. The concentration of each LDH was 50 ppm. The medium containing no LDH was used as the "control" medium. The cells were seeded at a density of 1000 cells per well in 96-well plates with the culture medium (control medium), followed by culturing for 24 h in a humidified incubator with 5% CO_2. The media were removed, and the CoAl-LDH-FA or CoAl-LDH containing medium was added in the 96-well plate. The media in each well were changed every other day. The number of cells in the 96-well plates was measured using the alamarBlue cell viability reagent (Thermo Fisher Scientific), following the instruction for the kit. Briefly, the alamarBlue reagent was mixed with the culture medium (control medium) with the ratio 1 : 10 (volume), then 110 μL of the mixed solution was added in each well and left in an incubator for 4 h. The metabolic activity of the cells was evaluated by measuring the fluorescence of the medium taken from each well with an excitation wavelength of 540 nm and emission wavelength of 590 nm using a multimode plate reader (EnSpire, PerkinElmer) (n = 4). The statistical significance was determined using the Tukey test ($p < 0.05$).

3. Results and discussion

FA, also known as pteroylglutamic acid, has been taken advantage of to target tumors since folate receptors are expressed on the surface of many human cancer cell types.[34,35] The pteroate moiety of folic acid is buried inside the receptor of cancer cells upon interaction, while its glutamate moiety is solvent-exposed and protrudes from the entrance of the pocket.[36] The configuration of FA interacting with the folate receptor implies that modification of LDH by FA through the carboxyl group of the glutamate moiety expectedly imparts the cancer-targeting capability to LDH. On the other hand, the FA modification through the carboxylic group is rarely reported. FA has been modified on materials through covalent bonding, namely, through a carbodiimide-mediated peptide coupling reaction in the presence of *N*-(3-dimethylaminopropyl)-*N*′-ethylcarbodiimide (EDC) and *N*-hydroxysuccinimide (NHS).[37–40] In the present study, the electrostatic interaction between the LDH platelet and the glutamic acid moiety was utilized as a weaker interaction to allow for controlling the release of Co^{2+} ion under mild conditions as well as targeting the properties of tumors (Fig. 1).

XRF analysis revealed that Co/Al ratios of CoAl-LDH and CoAl-LDH-FA are 2.02 and 1.98, respectively. The results suggest that chemical compositions are comparable for LDHs before and after the FA modification. Fig. 2a shows XRD patterns of CoAl-LDH and CoAl-LDH-FA. CoAl-LDH exhibits a typical XRD pattern of hydrotalcite type LDH. The diffraction patterns were preserved after the FA modification (CoAl-LDH-FA), suggesting that LDH crystals are intact due to the modification by FA. The 003 diffraction at 11.4° corresponding to d_{003} = 0.775 nm was comparable for both the samples, indicating that the modification of FA occurs on the surface of crystals without intercalation in interlayers; Xiao *et al.* reported the intercalation of folic acid results in the expansion of d_{003} values to 1.42 nm,[41,42] which is not the case in the present study. The surface modification of LDH nanoparticles with FA was further confirmed by FT-IR. Fig. 2b shows FT-IR spectra before and after the FA modification. The broad absorption band at 1600 cm^{-1} for CoAl-LDH appears as a result of overlapped

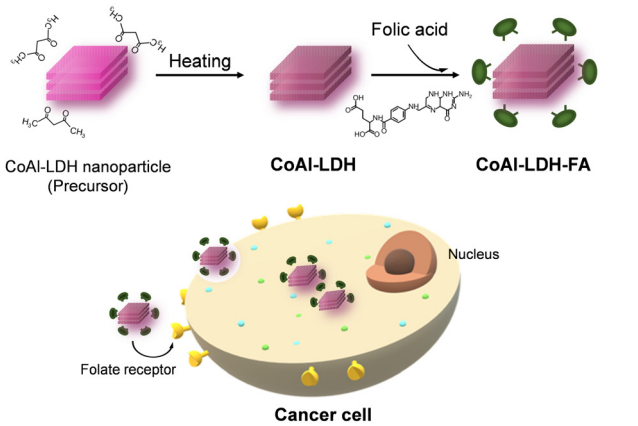

Fig. 1 A schematic showing the concept of the present materials synthesis.

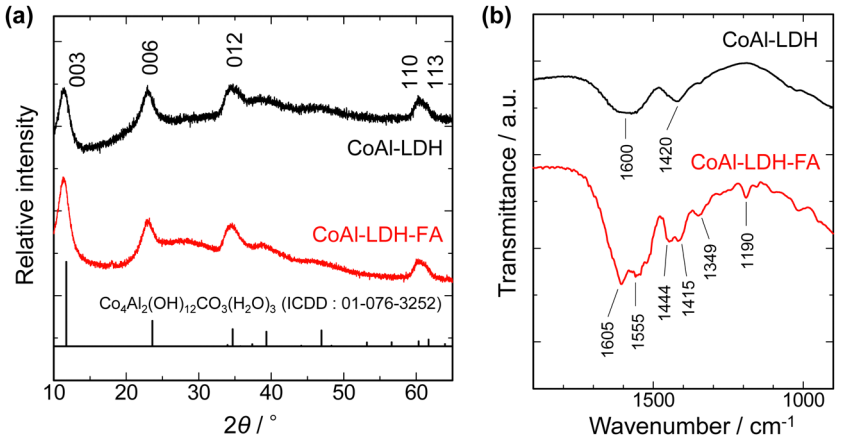

Fig. 2 (a) XRD patterns and (b) FTIR spectra of CoAl-LDH before and after folic acid modification.

peaks of OH stretching vibration, deformation vibration of the hydroxide basal layer, and interlayer water molecules. The peak of 1420 cm^{-1} is derived from the stretching vibration of CO_3^{2-} in interlayers.[43] In addition to these, some peaks observed on the spectrum of CoAl-LDH-FA are derived from FA[44,45] as follows: 1605 cm^{-1} and 1190 cm^{-1} for CN stretching vibrations of FA; 1555 cm^{-1} and 1349 cm^{-1} for antisymmetric and symmetric stretching vibration modes of carboxylic groups of FA ($\nu_{as}(COO^-)$ and $\nu_s(COO^-)$), respectively; peaks at 1444 cm^{-1} and 1415 cm^{-1} for bending vibration of CH_2 in FA. The peaks of $\nu_{as}(COO^-)$ and $\nu_s(COO^-)$ are shifted to lower wavenumbers from those of free-FA. The shift indicates the bidentate coordination of COO^- to metal centers of hydroxide layers according to the literature on a Co–FA metal complex.[44,46] The present configuration of coordination is in good agreement with the ones reported on transition metal hydroxides, such as $Ni(OH)_2$ and $Co(OH)_2$, modified with mono carboxylic acids including acrylic acid and acetic acid.[47–49]

The modification with FA was further quantitatively examined. Fig. 3 shows TG curves of CoAl-LDH and CoAl-LDH-FA. The samples exhibit weight loss explained by 3 phenomena: (i) <200 °C: desorption of physically adsorbed water; (ii) 250–350 °C: release of water from interlayers and/or condensation of OH groups to form oxides; (iii) >350 °C: decomposition of folic acid coordinated on the crystal surface. The range (ii) was observed at a relatively higher temperature for CoAl-LDH-FA, which reflects its higher thermal stability because of complexation with FA. The higher thermal stability is also suggested by the relatively higher decomposition temperature of folic acid; free folic acid rapidly decomposes at *ca.* 250 °C,[50] whereas in the present case it is suppressed up to *ca.* 350 °C. The nanometric shape with a high surface area allows for loading a large amount of FA. This is confirmed by the larger total weight loss for CoAl-LDH-FA, 53%, compared to CoAl-LDH, 39% at 900 °C. The larger weight loss for CoAl-LDH-FA also includes the contribution of DMSO incorporated through its interaction with FA. Even after the modification with FA, particles have a high surface charge advantageous for uptake into cancer cells; the zeta potentials at pH = 7.4 of CoAl-LDH and CoAl-LDH-FA are +29.1 and +35.9 mV, respectively.

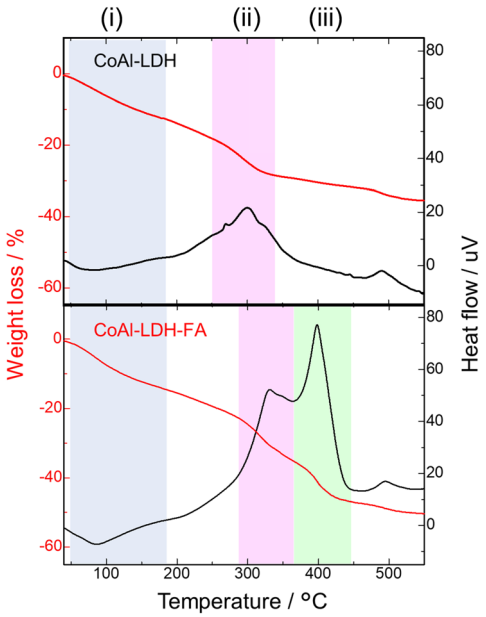

Fig. 3 TG and DTA curves of CoAl-LDH before and after folic acid modification; 3 successive phenomena accompanied by weight loss observed in (i)–(iii) temperature ranges.

A comparative study was conducted using highly crystalline large LDH platelets before and after FA modification (Ref-CoAl-LDH and Ref-CoAl-LDH-FA). Ref-CoAl-LDH was prepared according to a previous report by using urea as a alkalization agent (urea method).[32] BET surface areas estimated by N_2 adsorption–desorption measurement were 136 and 10 $m^2\ g^{-1}$ for CoAl-LDH and Ref-CoAl-LDH, respectively. While CoAl-LDH with nanometric shape keeps its original crystalline nature even after 250 °C, Ref-CoAl-LDH degrades and produces the impurity phase (Fig. S2a, ESI†). For this reason, FA modification was performed on Ref-CoAl-LDH without the thermal treatment. The crystalline nature and morphology of Ref-CoAl-LDH were intact even after the FA modification (Fig. S2b and c, ESI†). Nevertheless, TG-DTA and FT-IR measurements reveal that a negligible difference is observed for the samples before and after FA modification as

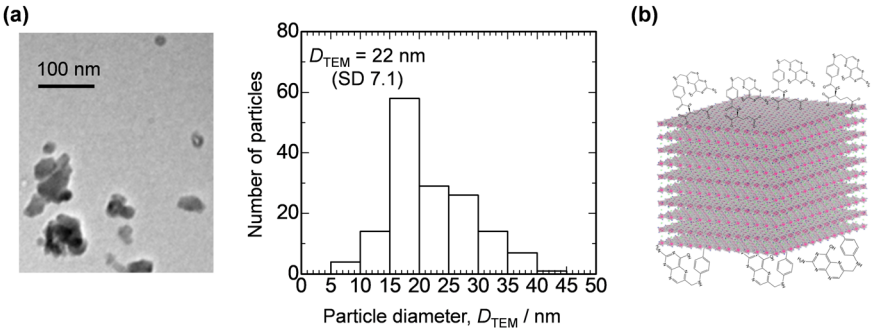

Fig. 4 (a) A representative TEM image and particle size distribution of CoAl-LDH-FA. (b) Schematic image showing CoAl-LDH-FA.

shown in Fig. S3a and b (ESI†). A detectable amount of loading of folic acid was not confirmed for Ref-CoAl-LDH presumably due to the low surface area and the low surface basicity.[51] It can be concluded that the small particle size and higher thermal stability of the CoAl-LDH sample allow for FA modification.

As the final part of the material characterization, the impact of FA modification on the morphological feature of LDH was assessed. Fig. 4a shows a representative TEM image and the corresponding particle size distribution of CoAl-LDH-FA. The primary particles of CoAl-LDH-FA exhibits an isotropic shape (low aspect ratio compared to general LDH platelets) and the average diameter of CoAl-LDH-FA was estimated at 22 nm. The size is comparable to or slightly larger than the one before modification. Taking into account all the above results of TEM, FTIR, TG-DTA, and XRD, we can conclude that the surface of nanometric CoAl-LDH was successfully decorated with FA (Fig. 4b).

There have been reports on systems allowing for the controlled release of molecules/ions by using LDH where LDH is used as a buffering material (alkaline solid) to respond and dissolve under acidic condition.[52,53] A precise pH response is also desirable for the CDT application. In particular, a sharp pH response around at pH = 7 is desirable because cancer cells exhibit an extracellular pH value as low as 6.5 which is relatively lower than that of normal cells ~7.4.[54] Fig. 5 shows Co^{2+} dissolution from CoAl-LDH and CoAl-LDH-FA in phosphate buffer solutions of varied pH values at 37 °C. As the concentration of LDH particles in the buffer solutions, C_{LDH}, increases from 20 ppm to 50 ppm, the dissolution of Co^{2+} is enhanced. Another clear trend is that FA modification suppresses the Co^{2+} dissolution at all the examined pH. The concentration of Co^{2+} dissolved from CoAl-LDH-FA at pH = 7.4 are comparable to IC50 for C_{LDH} = 20 and 30 ppm. These results reveal that FA on the crystal surface can slow down the dissolution of Co^{2+} at a given pH. The retarded dissolution of Co^{2+} would be due to the lower dissolution of FA to water. The complexation of FA with Co^{2+} on the surface of LDH prevents Co^{2+} from hydration by solvents thereby dissolution to aqueous media. In addition, dissolved Co^{2+}at the vicinity of LDH is expected to be trapped thorough coordination with abundant basic amines sites in the pteroate part, as reported for methotrexate (a folate analog).[55] This also contributes to the retarded dissolution of Co^{2+}.

As demonstrated above, the modification with FA occurs through a carboxylic moiety. Enhanced targeting properties utilizing the pteroate moiety as well as dissolution in cancer cells are highly expected. Finally, this possibility was assessed by metabolic activity tests for two different types of cells, mouse fibroblast-like cell line (NIH3T3) and human cell line derived from a cervical cancer (HeLa), after culturing with CoAl-LDH and CoAl-LDH-FA. NIH3T3 was used as a normal cell line, while HeLa was used as a cancer cell line. Fig. 6 shows the metabolic activity levels of each cell after culturing with CoAl-LDH and CoAl-LDH-FA. In the case of NIH3T3, their activity levels after culturing with CoAl-LDH was significantly lower than that of control at days 3 and 5, whereas the level after culturing with CoAl-LDH-FA was higher than that of CoAl-LDH at every time

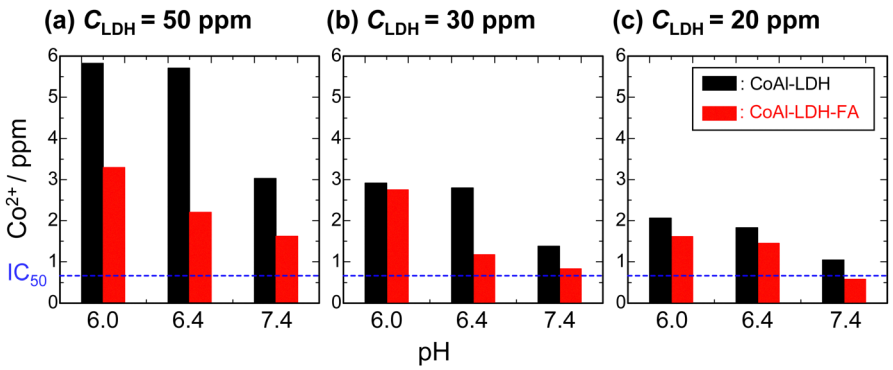

Fig. 5 Co^{2+} ion dissolution to buffer solutions of varied pH after incubation at 37 °C for 1 day. C_{LDH}: concentration of LDH initially added to buffer solutions. IC_{50}: the half maximal inhibitory inhibitive concentration for MC3T3-E1. IC_{50} = 0.66 ppm for Co^{2+}.

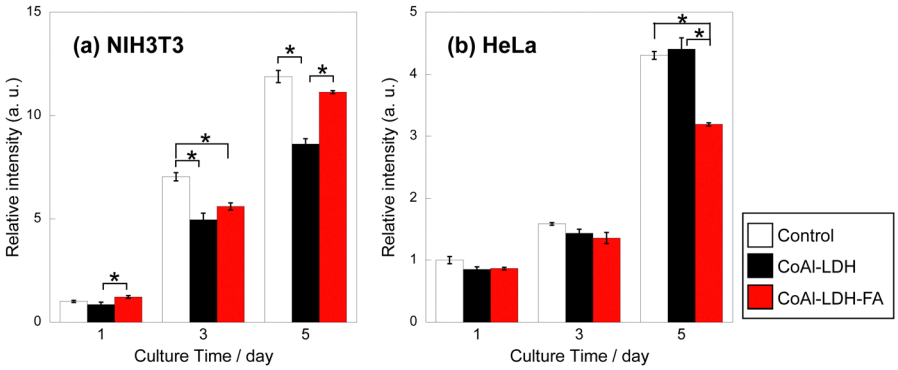

Fig. 6 Metabolic activity level of (a) NIH3T3 and (b) HeLa after culturing with CoAl-LDH and CoAl-LDH-FA. (*$p < 0.05$).

point and reached a similar value to that of control at day 5. The levels of HeLa possessed an opposite tendency with that of NIH3T3; the levels of the cells cultured with CoAl-LDH was similar to that of control, while the levels of CoAl-LDH-FA was significantly lower at day 5. These changes in the metabolic activity of the cells are expected to be related to Co^{2+} ions released from CoAl-LDH inside and outside of the cells. As mentioned above, the Co^{2+} ion dissolution of CoAl-LDH was controlled by the FA modification. A smaller amount of Co^{2+} ions should be released from CoAl-LDH-FA than CoAl-LDH outside the cells, which contributes to the higher activity level of the normal cell line, NIH3T3. On the other hand, in the case of the cancer cell line, HeLa, since the FA on CoAl-LDH enhances the cancer-cell-targeting property, a larger amount of CoAl-LDH-FA should attach on the surfaces of HeLa cells and some of them are taken up by the cells. The CoAl-LDH-FA on the surfaces and inside of the cells release Co^{2+} ions due to the acidic conditions, which induces the lower metabolic activity of the cells. Chung *et al.* reported that MgAl-LDH with 50 nm in size were internalized into cells and a part of the internalized one followed a typical endosome–lysosome pathway.[56] On the other hand, several papers reveal that cellular uptake of nanoparticles depends on their size. Oh *et al.* reported that MgAl LDH nanoparticles of 50–200 nm are internalized through a clathrin-mediated endocytosis, while a large particle of 350 nm was not selective in endocytic pathways.[57] In the investigations on gold nanoparticles[58] and mesoporous silica nanoparticles,[59] the maximum uptake by cells occurred for the nanoparticles around 50 nm in size and the uptake amount for <50 nm was larger than that for >100 nm. Therefore, a larger amount of CoAl-LDH-FA might be taken up by HeLa and degraded through the endosome–lysosome pathway because of their size of 22 nm, which could contribute to the change in the cell functions. Thus, CoAl-LDH-FA exhibits both the smaller cytotoxicity to normal cells and the targeting and killing properties against cancer cells.

As discussed in Fig. 2, the interlayer spaces of present CoAl LDH nanoparticles are intact and not exchanged with FA molecules. This offers further possibility to accommodate functional organic molecules. In addition, LDH nanomaterials have been reported to be used as nano building blocks for constructing functional nanocomposites.[48] These potential advantages of using the present materials further will create opportunities for their use as adaptive nanomaterials.

4. Conclusions

We have demonstrated a facile synthesis route toward 20-nm-sized CoAl LDH nanoparticles modified with folic acid. XRD measurements revealed that the modification of FA occurs on the surface of crystals without intercalation in interlayers. FT-IR analysis suggests bidentate coordination of COO^- to metal centers of hydroxide layers, between the glutamate moiety of folic acid and CoAl LDH. The relatively weak interaction allowed for controlled dissolution of LDH nanoparticles in a pH-responsive manner. The concentration of Co^{2+} dissolved from CoAl-LDH-FA at pH = 7.4 is comparable to IC50 for C_{LDH} = 20 and 30 ppm. These results reveal that FA on the crystal surface can slow down the dissolution of Co^{2+} at a given pH. Cell culture tests suggest that the materials exhibit targeting properties towards cancer cells to enhance cellular uptake. As a result, lowered metabolic activity was induced for the cancer cell line. Thanks to the chemical versatility and morphological tunability of LDHs, the nanometric LDH-based materials demonstrated in the present study are expected to find applications as adaptive nanomaterials in the biological field.

Author contributions

Conceptualization: Y. T. and A. O.; investigation: N. K., K. N., E. G., Y. M., and Y. K.; writing (original draft): Y. T., and A. O.; writing (review and editing): N. K., H. M., A. N., and T. K.; funding acquisition: Y. T. and A. N.; Validation: N. K.

Conflicts of interest

There are no conflicts to declare.

Acknowledgements

The present work is partially supported by the JSPS KAKENHI (Grant Number JP20H02442), Grant-in-Aid for Scientific

Research on Innovative Areas, Grant for Science Research from Takahashi Industrial and Economic Research Foundation.

References

1 Z. Tang, Y. Liu, M. He and W. Bu, *Angew. Chem., Int. Ed.*, 2019, **58**, 946–956.
2 H. Lin, Y. Chen and J. Shi, *Chem. Soc. Rev.*, 2018, **47**, 1938–1958.
3 L. S. Lin, J. Song, L. Song, K. Ke, Y. Liu, Z. Zhou, Z. Shen, J. Li, Z. Yang, W. Tang, G. Niu, H. H. Yang and X. Chen, *Angew. Chem., Int. Ed.*, 2018, **57**, 4902–4906.
4 A. D. Bokare and W. Choi, *J. Hazard. Mater.*, 2014, **275**, 121–135.
5 S. Wang, F. Li, R. Qiao, X. Hu, H. Liao, L. Chen, J. Wu, H. Wu, M. Zhao, J. Liu, R. Chen, X. Ma, D. Kim, J. Sun, T. P. Davis, C. Chen, J. Tian, T. Hyeon and D. Ling, *ACS Nano*, 2018, **12**, 12380–12392.
6 Y. Wang, W. Wu, J. Liu, P. N. Manghnani, F. Hu, D. Ma, C. Teh, B. Wang and B. Liu, *ACS Nano*, 2019, **13**, 6879–6890.
7 L. Yang, X. J. Zhu, M. Qu, T. R. Xu, Y. M. Ye, Z. Z. Zeng, J. Zhang, L. K. Wang, Z. P. Yu and H. P. Zhou, *ACS Appl. Bio. Mater.*, 2021, **4**, 4507–4521.
8 X. Cheng, H. D. Xu, H. H. Ran, G. Liang and F. G. Wu, *ACS Nano*, 2021, **15**, 8039–8068.
9 X. Shi, N. S. Dalai and K. S. Kasprzak, *Chem. Res. Toxicol.*, 1993, **6**, 277–283.
10 C. P. Lewis, M. Demedts and B. Nemery, *Am. J. Respir. Cell Mol. Biol.*, 1991, **5**, 163–169.
11 V. Rives, *Layered Double Hydroxides: Present and Future*, Nova Science Publishers, Inc, New York, 2001.
12 I. T. Sherman, *Layered Double Hydroxides (LDHs): Synthesis, Characterization and Applications*, Nova Science Publishers, Inc, New York, 2015.
13 L. Yan, Y. Wang, T. Hu, X. Mei, X. Zhao, Y. Bian, L. Jin, R. Liang, X. Weng and M. Wei, *J. Mater. Chem. B*, 2020, **8**, 1445–1455.
14 X. Yang, L. Wang, S. Guo, R. Li, F. Tian, S. Guan, S. Zhou and J. Lu, *Adv. Healthcare Mater.*, 2021, **10**, 2100539.
15 Z. Wang, L. Fu, Y. Zhu, S. Wang, G. Shen, L. Jin and R. Liang, *J. Mater. Chem. B*, 2021, **9**, 710–718.
16 T. Hu, L. Yan, Z. Wang, W. Shen, R. Liang, D. Yan and M. Wei, *Chem. Sci.*, 2021, **12**, 2594–2603.
17 J. Lu, Z. Guo, S. Che, F. Gao, Z. Gu, J. Xu, Y. Chi, W. Xu, J. Zhang, N. Takuya, J. Yu and L. Zhao, *J. Mater. Chem. B*, 2020, **8**, 11082–11089.
18 T. Jia, Z. Wang, Q. Sun, S. Dong, J. Xu, F. Zhang, L. Feng, F. He, D. Yang, P. Yang and J. Lin, *Small*, 2020, **16**, 2001343.
19 Q. Wang and D. O'Hare, *Chem. Rev.*, 2012, **112**, 4124–4155.
20 R. Sasai, H. Sato, M. Sugata, T. Fujimura, S. Ishihara, K. Deguchi, S. Ohki, M. Tansho, T. Shimizu, N. Oita, M. Numoto, Y. Fujii, S. Kawaguchi, Y. Matsuoka, K. Hagura, T. Abe and C. Moriyoshi, *Inorg. Chem.*, 2019, **58**, 10928–10935.
21 D. Kino, Y. Tokudome, P. D. Vaz, C. D. Nunes and M. Takahashi, *J. Asian Ceramic Soc.*, 2017, **5**, 466–471.
22 K. Wang, L. Zhang, Y. Su, D. Shao, S. Zeng and W. Wang, *J. Mater. Chem. A*, 2018, **6**, 8366–8373.
23 Y. Zhang, D. Du, X. Li, H. Sun, L. Li, P. Bai, W. Xing, Q. Xue and Z. Yan, *ACS Appl. Mater. Interfaces*, 2017, **9**, 31699–31709.
24 Z. Liu, L. Teng, L. Ma, Y. Liu, X. Zhang, J. Xue, M. Ikram, M. Ullah, L. Li and K. Shi, *RSC Adv.*, 2019, **9**, 21911–21921.
25 J. Han, Y. Dou, J. Zhao, M. Wei, D. G. Evans and X. Duan, *Small*, 2013, **9**, 98–106.
26 N. S. Ahmed, R. Menzel, Y. Wang, A. Garcia-Gallastegui, S. M. Bawaked, A. Y. Obaid, S. N. Basahel and M. Mokhtar, *J. Solid State Chem.*, 2017, **246**, 130–137.
27 M. Luo, M. Li, B. Lü, Q. Liu, Z. Di and L. Guo, *ACS Appl. Nano Mater.*, 2021, **4**, 3734–3741.
28 Y. Wang, X. Dai, Q. Zhou, K. Li, L. Feng, W. Liao, Y. Yu, H. Yu, X. Zong, G. Lu and Y. Zhang, *Colloids Surf., A*, 2022, 636.
29 V. Oestreicher, I. Fabregas and M. Jobbagy, *J. Phys. Chem. C*, 2014, **118**, 30274–30281.
30 I. R. Younis, M. K. Stamatakis, P. S. Callery and P. J. Meyer-Stout, *Int. J. Pharm.*, 2009, **367**, 97–102.
31 Z. Wu, X. Li, C. Hou and Y. Qian, *J. Chem. Eng. Data*, 2010, **55**, 3958–3961.
32 Z. Liu, R. Ma, M. Osada, N. Iyi, Y. Ebina, K. Takada and T. Sasaki, *J. Am. Chem. Soc.*, 2006, **128**, 4872–4880.
33 T. Haraguchi, T. Okuno, H. Nishikawa, H. Kojima, S. Ikegami, M. Yoshida, M. Habara, H. Ikezaki and T. Uchida, *Chem. Pharm. Bull.*, 2019, **67**, 1271–1277.
34 A. C. Antony, *Blood*, 1992, **79**, 2807–2820.
35 S. Wen, H. Liu, H. Cai, M. Shen and X. Shi, *Adv. Healthcare Mater.*, 2013, **2**, 1267–1276.
36 C. Chen, J. Ke, X. Edward Zhou, W. Yi, J. S. Brunzelle, J. Li, E. L. Yong, H. E. Xu and K. Melcher, *Nature*, 2013, **500**, 486–489.
37 F. Yin, B. Zhang, S. Zeng, G. Lin, J. Tian, C. Yang, K. Wang, G. Xu and K. T. Yong, *J. Mater. Chem. B*, 2015, **3**, 6081–6093.
38 B. Sahoo, K. S. P. Devi, R. Banerjee, T. K. Maiti, P. Pramanik and D. Dhara, *ACS Appl. Mater. Interfaces*, 2013, **5**, 3884–3893.
39 S. Rana, N. G. Shetake, K. C. Barick, B. N. Pandey, H. G. Salunke and P. A. Hassan, *Dalton Trans.*, 2016, **45**, 17401–17408.
40 Z. Wang, D. Shao, Z. Chang, M. Lu, Y. Wang, J. Yue, D. Yang, M. Li, Q. Xu and W. F. Dong, *ACS Nano*, 2017, **11**, 12732–12741.
41 R. Xiao, W. Wang, L. Pan, R. Zhu, Y. Yu, H. Li, H. Liu and S. L. Wang, *J. Mater. Sci.*, 2011, **46**, 2635–2643.
42 T. H. Kim and J. M. Oh, *J. Solid State Chem.*, 2016, **233**, 125–132.
43 D. Tichit, M. H. Lhouty, A. Guida, B. H. Chiche, F. Figueras, A. Auroux, D. Bartalini and E. Garrone, *J. Catal.*, 1995, **151**, 50–59.
44 M. G. A. El-Wahed, M. S. Refat and S. M. El-Megharbel, *Spectrochim. Acta, Part A*, 2008, **70**, 916–922.
45 M. Baibarac, I. Smaranda, A. Nila and C. Serbschi, *Sci. Rep.*, 2019, **9**, 14278.
46 F. Jiang, H. Ye, H. Li, K. Sun, J. Yin and H. Zhu, *Chem. Commun.*, 2018, **54**, 4971–4974.
47 N. Tarutani, Y. Tokudome, M. Jobbágy, G. J. A. A. Soler-Illia, Q. Tang, M. Müller and M. Takahashi, *Chem. Mater.*, 2019, **31**, 322–330.
48 N. Tarutani, Y. Tokudome, M. Jobbágy, G. J. A. A. Soler-Illia and M. Takahashi, *J. Mater. Chem. A*, 2019, **7**, 25290–25296.

49 N. Tarutani, Y. Tokudome, M. Jobbágy, F. A. Viva, G. J. A. A. Soler-Illia and M. Takahashi, *Chem. Mater.*, 2016, **28**, 5606–5610.
50 A. Vora, A. Riga, D. Dollimore and K. S. Alexander, *Thermochim. Acta*, 2002, **392–393**, 209–220.
51 Y. Tokudome, M. Fukui, S. Iguchi, Y. Hasegawa, K. Teramura, T. Tanaka, M. Takemoto, R. Katsura and M. Takahashi, *J. Mater. Chem. A*, 2018, **6**, 9684–9690.
52 Q. Zheng, Y. Hao, P. Ye, L. Guo, H. Wu, Q. Guo, J. Jiang, F. Fu and G. Chen, *J. Mater. Chem. B*, 2013, **1**, 1644–1648.
53 S. Senapati, T. Sarkar, P. Das and P. Maiti, *Bioconjugate Chem.*, 2019, **30**, 2544–2554.
54 M. Damaghi, J. W. Wojtkowiak and R. J. Gillies, *Front. Phys.*, 2013, **4**, 370.
55 H. J. Kim, J. Y. Lee, T. H. Kim, G. H. Gwak, J. H. Park and J. M. Oh, *Appl. Clay Sci.*, 2020, **186**, 105454.
56 H. E. Chung, D. H. Park, J. H. Choy and S. J. Choi, *Appl. Clay Sci.*, 2012, **65–66**, 24–30.
57 J. M. Oh, S. J. Choi, G. E. Lee, J. E. Kim and J. H. Choy, *Chem.–Asian J.*, 2009, **4**, 67–73.
58 B. D. Chithrani, A. A. Ghazani and W. C. W. Chan, *Nano Lett.*, 2006, **6**, 662–668.
59 F. Lu, S. H. Wu, Y. Hung and C. Y. Mou, *Small*, 2009, **5**, 1408–1413.